CEAS Aeronautical Journal
https://doi.org/10.1007/s13272-026-00966-y

ORIGINAL PAPER

Numerical interpretation of whirl flutter in a tiltrotor wind-tunnel model using mid-fidelity aerodynamics and mechanical friction

Paolo De Vita[1] · Gianni Cassoni[1] · Marco Morandini[1] · Pierangelo Masarati[1] · Federico Fonte[2] · Marco Favale[2] · Stefan van't Hoff[3]

Received: 17 December 2025 / Revised: 13 March 2026 / Accepted: 30 March 2026

Abstract

This paper investigates the aeroelastic stability of the ATTILA tiltrotor wind-tunnel testbed through numerical modeling of the system's advanced dynamic characteristics. Specifically, the study addresses discrepancies between baseline predictions and experimental observations regarding the unexpected sensitivity of flutter modes' damping to rotor disk tilting. Two enhancements are explored: mid-fidelity aerodynamic modeling using vortex particle methods and mechanical friction modeling in critical joints. Vortex particle free wake and vortex lattice-based modeling for wing aerodynamics significantly improve damping predictions for the out-of-plane bending and torsion modes compared to strip theory approaches for the wing and rotor blades. In contrast, modeling rotor aerodynamics with lifting line and vortex particle free wake only shows marginal improvements. However, aerodynamic enhancements alone cannot reproduce the experimentally observed sensitivity to the gimbal angle. Conversely, introducing friction in specific joints can qualitatively replicate the observed tilt-dependent behavior through stiction-induced joint locking.

Keywords Tiltrotor · Whirl-flutter · Vortex-particle aerodynamics · Fluid–structure interaction · Friction

1 Introduction

Tiltrotor aircraft combine vertical take-off and landing capabilities with efficient high-speed cruise. This is achieved thanks to their unique configuration that enables the rotation of wing-mounted rotors, allowing the aircraft to convert from helicopter to airplane mode. While offering remarkable capabilities, the design of a tilting nacelle introduces significant engineering challenges, particularly concerning aeroelastic stability across the entire flight envelope. An aeroelastic instability known as whirl flutter can be a limit for the cruise speed of tiltrotor aircraft. Whirl flutter arises from the interaction between rotor aerodynamic forces and the elastic modes of the structure the rotor is mounted on. The fundamental mechanism behind whirl flutter instability is the gyroscopic effect, where the rotation of the rotor disk couples different degrees of freedom of the structure, adding a stabilizing or destabilizing influence depending on the frequency and phase relationships of the involved oscillations.

Whirl flutter has been a focal point of rotorcraft research since the early tiltrotor studies of the 1980s, during which extensive experimental and numerical modeling work was carried out for the development of the JVX/V-22 tiltrotor

✉ Pierangelo Masarati
pierangelo.masarati@polimi.it

Paolo De Vita
paolo.devita@mail.polimi.it

Gianni Cassoni
gianni.cassoni@polimi.it

Marco Morandini
marco.morandini@polimi.it

Federico Fonte
federico.fonte@leonardo.com

Marco Favale
marco.favale@leonardo.com

Stefan van't Hoff
stefan.van.t.hoff@nlr.nl

[1] Department of Aerospace Science and Technology, Politecnico di Milano, Via La Masa 34, 20156 Milan, Italy

[2] Rotor Aeroelasticity, Leonardo Helicopters, Via Giovanni Agusta 520, 21017 Cascina Costa di Samarate, VA, Italy

[3] Rotorcraft Aeromechanics, Royal Netherlands Aerospace Centre, Anthony Fokkerweg 2, 1059 CM Amsterdam, Netherlands

Published online: 13 April 2026

[1–7]. In Europe, in the early 2000s, the ERICA concept [8] explored an original tiltrotor configuration. Its aeroelastic stability was addressed by projects like ADYN (6th Framework Programme, [9, 10]) and NICETRIP (7th Framework Programme, [11]), which progressed to the aeroelastic wind-tunnel testing stage. More recently, the US Army has renewed its commitment to advancing the understanding of tiltrotor whirl flutter by commissioning the TRAST testbed, an effort intended to address limitations in earlier test campaigns related to uncertainties in dynamic and aerodynamic properties, inconsistencies in recorded data, and restricted data accessibility [12–18]. A further contemporary initiative focused on experimental characterization of tiltrotor whirl flutter is currently underway at the University of Maryland in collaboration with NASA Ames Research Center [19–21]. In parallel, researchers at the Georgia Institute of Technology are investigating new approaches to analyze the whirl-flutter stability of nonlinear systems [22].

The Clean Sky 2 initiative is a major European research program that has enabled the development of innovative aviation technologies to reduce greenhouse gas—mainly CO_2—emissions, noise, and pollutants from aircraft. As part of this initiative, the Next Generation Civil TiltRotor (NGCTR) project was aimed at pushing the technological boundaries of tiltrotor aircraft. A design objective of the NGCTR was to enhance cruise efficiency by employing thinner wing sections, which reduced the torsional stiffness, creating new challenges in maintaining sufficient whirl flutter stability margins while optimizing aerodynamic performance and structural weight. To address these challenges, the Advanced Testbed for TILtrotor Aeroelastics (ATTILA) project, coordinated by the Dutch Aerospace Research Center (NLR) with the participation of Leonardo Helicopters (LHD) and, among others, of Politecnico di Milano (POLIMI), was established as one of the main supporting initiatives for the NGCTR, focusing on developing, building, and testing [23] an advanced aeroelastic wind tunnel testing platform to validate the tiltrotor's design before flight testing through wind tunnel tests in both Froude and Mach scaled conditions.

Results from testing in the German-Dutch Wind Tunnels (DNW) Large Low-speed Facility (LLF) revealed discrepancies between numerical predictions and experimental results [24]. In particular, the main modes—wing out-of-plane and in-plane bending, and torsion—exhibited an unexpected sensitivity to the tilting of the rotor disk, and the torsional mode demonstrated higher than predicted whirl flutter speeds. This work, derived from a paper originally presented at the 51st European Rotorcraft Forum [25], and itself a substantial development of [26], analyzes recent modeling enhancements aimed at improving the correlation between simulations and experimental observations.

Section 2 outlines the wind tunnel testbed, numerical methodologies, and solvers. Section 3 analyzes the influence of mid-fidelity aerodynamic modeling of the wing and rotor on whirl-flutter predictions. Section 4 introduces friction models in selected system joints and presents a statistical assessment of their impact on aeroelastic stability. The main conclusions are summarized in Sect. 5.

2 Wind tunnel testbed and numerical models

The ATTILA wind tunnel testbed, shown in Fig. 1, consists of a 1:5 scale semi-span wing with a powered proprotor that replicates the design of the Next Generation Civil TiltRotor (NGCTR) developed by LHD. The model maintains dynamic similarity with the full-scale aircraft by adhering to Froude scaling. The testbed features a three-bladed 2.5 m diameter stiff in-plane rotor mounted on a 1.6 m cantilevered wing. The rotor connects to the mast through a gimbal joint, allowing for tilting of the rotor disk, while the blades are controlled by a control chain capable of both cyclic and collective commands. The mast, which is part of the tilting nacelle, connects to the non-tilting nacelle via a set of interchangeable springs designed to simulate both on-downstop and off-downstop conditions. The non-tilting nacelle attaches to the wing tip through a six-component load balance whose stiffness is a key element for tuning the dynamic behavior of the structure (Fig. 2, 3, 4).

The development of the project was supported by several aeroelastic and structural dynamics simulations, performed using CAMRAD II (LHD), FLIGHTLAB (NLR), and MBDyn (POLIMI), in strict cooperation and with frequent correlations, especially in terms of structural dynamics (i.e., predicted structural properties, see [27], and correlation with ground vibration test (GVT) results in preparation of wind-tunnel testing, see [28]), to match the actual hardware's development [23, 24, 29, 30]. The GVT setup is illustrated in Fig. 2, adapted from Fig. 5 of [28]. The MBDyn model used in this work, derived from the one presented in [30], is discussed in detail in the following, specifically addressing the modeling enhancements developed for the proposed investigation.

2.1 MBDyn structural and baseline aerodynamic model

A reference aeroelastic model of the ATTILA testbed was built using MBDyn to support its design and development phases [29, 30]. MBDyn[1] [31] is a free, general-purpose

[1] https://www.mbdyn.org/, last accessed December 2025.

Fig. 1 ATTILA testbed in the DNW Large Low-speed Facility (LLF) 6 m × 6 m wind tunnel test section

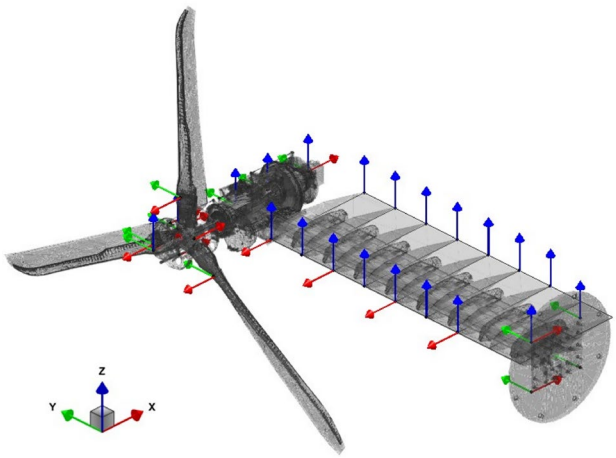

Fig. 2 ATTILA testbed GVT measurement setup

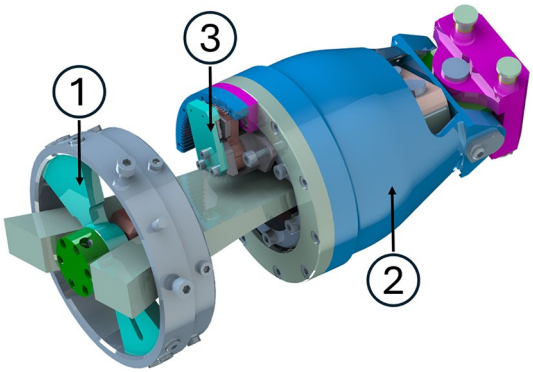

Fig. 3 CAD model of the pitch bearings (inner, 1, and outer, 2) and encoder (3)

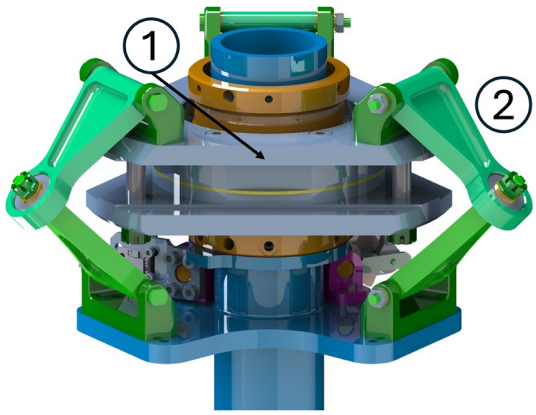

Fig. 4 CAD model of the gimbal joint assembly (yoke, 1, and compasses, 2)

multibody solver designed to simulate complex mechanical systems. The robustness of its implementation makes it suitable for applications ranging from simple mechanical systems to complex aeronautical structures. It has been widely used in research related to tiltrotor aircraft and whirl flutter [5, 30, 32–41].Notably, in [5], the experimental evidence of an unexpected damping trend in a soft-inplane configuration of the Wing and Rotor Aeroelastic Test System (WRATS) was explained by the observed backlash in the drivetrain of the powered wind-tunnel model when operating in windmill conditions, thus in a configuration that entailed repeated switching between positive and negative torque in the drive system, demonstrating the capabilities of MBDyn and multibody analysis for this kind of application.

The complete structure can be divided into two major components: the wing-pylon assembly and the rotor. The

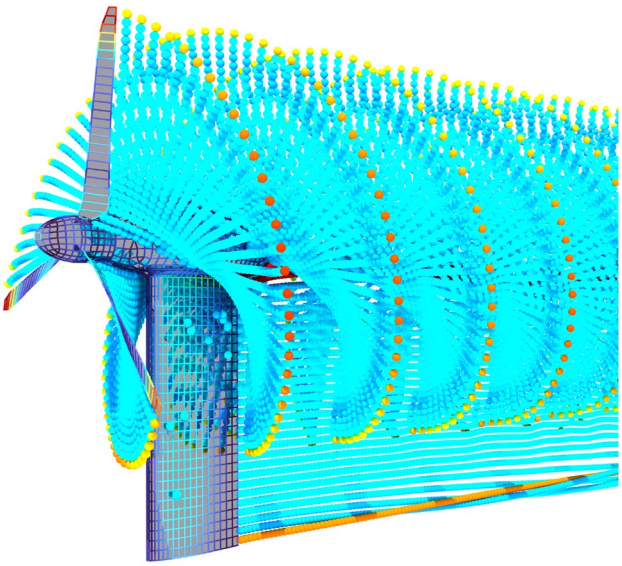

Fig. 5 Example of the DUST aerodynamic surfaces and wake on the ATTILA model

wing-pylon assembly comprises the wing, nacelle, and motor, while the rotor model consists of a yoke, the control chain, and three blades.

The structural model of the wing incorporates a series of finite-volume three-node beams based on C^0 kinematics [42, 43]. These one-dimensional structural components account for the viscoelastic properties of the structure. The inertial properties of the wing are condensed into a series of lumped masses for the airfoil segments, with additional non-structural masses strategically placed during the development of the wind tunnel model's design to match the system's target weight distribution of the wing, including the fuel. In the baseline analysis, the aerodynamic surface of the wing utilizes what in MBDyn's terminology are called 'aerodynamic beam' elements, which implement a two-dimensional strip theory model (corresponding to the Blade Element (BE) aerodynamic model in the context of a rotor blade [44]) relying on the deformation geometry and kinematics of the underlying three-node structural beam element. The two-dimensional aerodynamic load calculations incorporate C81 lookup tables to account for compressibility and viscosity effects.

The pylon, consisting of a nacelle and motor, connects the wing to the rotor. The nacelle is divided into non-tilting and tilting sections. The non-tilting nacelle is clamped to the wing tip and constrained to the tilting section through a downstop spring. This spring can be activated or deactivated during simulations to accommodate various experimental configurations, as the physical model allows for the substitution of the flexible downstop spring with a much stiffer, ideally rigid element. The nacelle structure is modeled as a flexible beam using three-node beam elements. The engine, clamped to the nacelle beam, is represented by a short beam section with strategically placed lumped bodies to accurately capture its dynamic behavior.

The rotor assembly comprises three blades, a yoke, and the control chain. Yoke and blades are modeled as flexible elements using the above-mentioned three-node beams. The blades connect to the yoke through inner and outer bearings (Fig. 3): the inner bearing (point 1) constrains the flapwise and chordwise displacement components, while the outer bearing (point 2) restricts all three displacement components; together, they only allow blade pitch rotation. The yoke is connected to the mast through a gimbal joint (Fig. 4), which allows rotor disk tilting while transferring axial rotation between the mast and the yoke.

The ATTILA structural model incorporates a complete helicopter-like control chain comprising three primary commands: cyclic, collective, and engine control. The cyclic control, both longitudinal and lateral, modifies the angle of attack of the blades as a function of the azimuth angle by rotating the swashplate about axes perpendicular to the mast. The collective control simultaneously adjusts the angle of attack of all blades by the same amount. Translation of the collective head along the mast axis alters blade angles through the pitch-link rods. The engine control involves applying a specific torque or angular velocity to the mast axis.

In the baseline model, the aerodynamics of the rotor blades utilize MBDyn's previously mentioned built-in aerodynamic beams where surfaces are defined with chord, twist, and (discretized) airfoil distributions along the spanwise direction, and deformation geometry and kinematics are inherited from the underlying beam elements. Sweep and dihedral angles are incorporated into the aerodynamic center position definition within the MBDyn nodes, eliminating the need for explicit specification in the aerodynamic beam definition. As for the wing, the aerodynamic loads are calculated using the blade element model based on C81 lookup tables specific to each rotor profile, with the addition of momentum theory to account for rotor inflow, in what is known as the blade element-momentum theory (BEMT) [44].

2.2 DUST aerodynamic model

DUST[2] is an open-source CFD tool that balances accuracy and computational efficiency, ideal for non-conventional configurations. It uses incompressible potential flow with compressibility corrections through aerodynamic elements and lookup tables. Its key feature is the use of the vortex particle method (VPM), a grid-free Lagrangian approach

[2] https://www.dust-project.org/, last accessed December 2025.

that enables the meshless representation of the wake, efficiently capturing the wake's effect on aerodynamic loads and its interactions with the aerodynamic surfaces. DUST can be tightly coupled to MBDyn using preCICE [45]. It offers three primary aerodynamic elements for representing physical bodies: Lifting Line (LL), Vortex Lattice (VL), and Surface Panels (SP).

2.2.1 Lifting line (LL)

The lifting line provides a one-dimensional representation for thin, slender lifting bodies, modeling them as a single row of vortex lattice panels with uniform doublet distribution. This element calculates principal aerodynamic coefficients (C_l, C_d, C_m) based on angle of attack (α), Reynolds number (Re), and Mach number (Ma). The LL method evaluates circulation intensity using tabulated aerodynamic data and employs a Γ-method for solving the nonlinear problem that equalizes lift predicted by the Kutta-Joukowski theorem with lift derived from aerodynamic data tables. While offering excellent numerical performance through its explicit numerical scheme, this approach may be susceptible to numerical instabilities.

2.2.2 Vortex lattice (VL)

The vortex lattice provides a two-dimensional representation of thin planar lifting surfaces by discretizing the mean line of airfoils into rectangular panels. Each panel contains a bound vortex with constant circulation. The VL method enforces the non-penetration boundary condition at collocation points to build a linear system for determining vortex intensities. Through this system, the circulation distribution across the surface can be determined, enabling the calculation of aerodynamic properties. The VL approach utilizes an implicit numerical scheme that ensures algorithmic stability at the cost of computational efficiency. It accounts for compressibility through the Prandtl-Glauert correction, but cannot capture nonlinear aerodynamic behaviors.

2.2.3 Surface panels (SP)

Surface panels discretize both lifting and non-lifting surfaces, making them ideal for modeling bodies where three-dimensional effects are significant. Based on the Boundary Element Method (BEM) originally proposed by Morino [46], this approach applies non-penetration boundary conditions directly on the actual surface. The SP method employs an implicit numerical scheme that provides greater accuracy at the cost of computational efficiency. While it handles complex geometries with higher fidelity, the method faces challenges with convergence and, like the vortex lattice approach, cannot represent nonlinear aerodynamic behaviors.

Figure 5 shows the most sophisticated and complete setup used for the coupled MBDyn/DUST simulations, i.e., lifting line for the rotor blades and vortex lattice for wing and nacelle surface panels, with vortex-particle free wake.

3 Whirl flutter prediction

The prediction of whirl flutter instabilities in tiltrotor aircraft traditionally relies on linearized aeroelastic models, where stability boundaries are determined through eigenvalue analysis. However, as noted, for example, in the work by Cocco et al. [30], this approach becomes problematic when modeling the system with multibody solvers formulated in the absolute reference frame. The difficulty stems from the inherent time-variant nature of rotorcraft dynamics, where the flow interaction with the rotor introduces periodicity in the system's response. To avoid this problem, a virtual experiment approach was adopted, simulating the process used in experimental testing campaigns. Like the above-mentioned approaches, this methodology relies on the assumption that for small perturbations around an equilibrium condition, the system's response can be approximated as locally linear, allowing for the characterization of each mode through its frequency and damping ratio extracted from carefully designed excitation and free-response analysis. The procedure consists of three principal phases:

First, modal identification is performed through broadband excitation using a linear chirp signal (the frequency varies linearly with time). The resulting response is analyzed using continuous wavelet transforms (CWT), revealing the system's natural frequencies at each specific trim condition.

Following modal identification, targeted excitation is applied for each mode of interest using sinusoidal forcing at the identified natural frequencies. The excitation amplitude is carefully calibrated to exceed the numerical noise floor while remaining within the quasi-linear response regime. In experiments, the excitation amplitude is often tuned to maintain roughly the same internal loads across different speeds, for safety considerations. The system is then allowed to respond freely after the excitation stops.

Finally, frequency and damping ratio are extracted from the free response using the Matrix Pencil Estimation (MPE) method [47]. This technique represents the signal as a linear combination of complex exponential terms, enabling the accurate identification of modal parameters from the decay signature. For the accurate extraction of the modal parameters, noise reduction methods such as SVD decomposition [48] and appropriate signal filtering are of paramount importance. The resulting frequencies from the MPE

identification are then used for subsequent excitation of the structure. This iterative process continues until the excitation frequency converges sufficiently close to the identified frequency.

From this analysis, three principal structural modes were identified as critical for whirl flutter prediction: the beamwise (out-of-plane wing bending), chordwise (in-plane wing bending), and torsional modes. Whirl flutter is predicted when the damping ratio of any mode approaches zero, signifying the onset of aeroelastic instability. This approach leverages computational simulation as a virtual laboratory for providing a data-based linearized model, enabling comprehensive stability analysis across the operational envelope while circumventing the limitations of a priori linearized models in capturing complex aeroelastic phenomena.

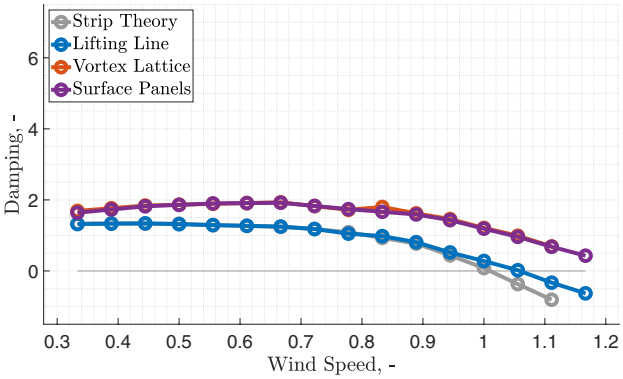

(a) Beamwise mode damping.

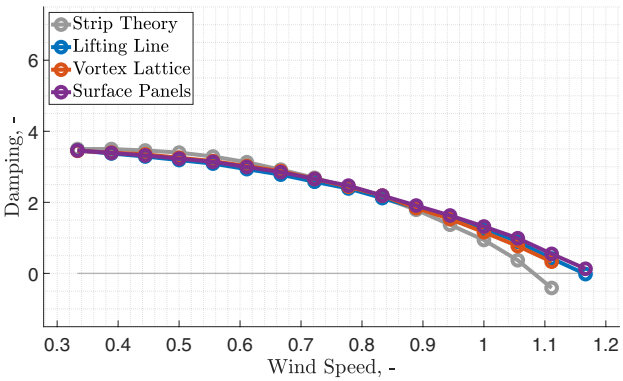

(b) Chordwise mode damping.

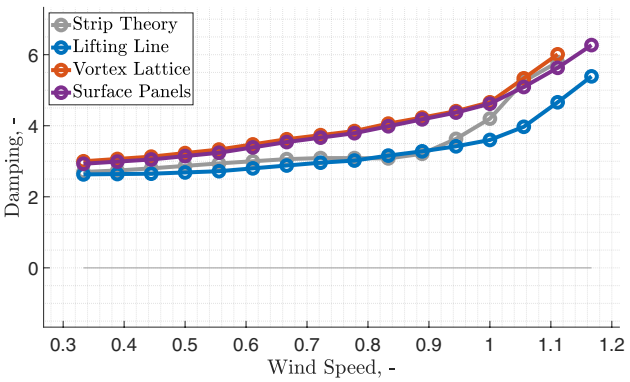

(c) Torsion mode damping.

Fig. 6 Comparison of damping ratios for different models of wing aerodynamics and lifting line for rotor aerodynamics

3.1 Model comparison

The investigation begins with a comparative analysis between the reference MBDyn model and the mid-fidelity DUST implementation to determine whether the Vortex Particle Method (VPM) improves whirl flutter predictions.

For this comparison, the MBDyn model using strip theory and blade element-momentum theory with tabulated airfoil data serves as the baseline. The DUST models maintain a consistent representation of the rotor aerodynamics using Lifting Line (LL) elements while implementing three distinct approaches for modeling the wing aerodynamics: Lifting Line (LL), Vortex Lattice (VL), and Surface Panels (SP).

Wing aerodynamics is sometimes neglected in whirl-flutter studies because omitting it typically yields conservative flutter speed estimates. In line with this common practice, preliminary analyses of the isolated wing indicated that including aerodynamic forces provides a substantial damping increase (approximately 2.1%-−2.5% for the beamwise bending mode) compared to a purely structural model, without significantly affecting the natural frequency. Since the present work focuses on interpreting experimental results where wing aerodynamics is inherently present, the separate impact of rotor aerodynamic models in the absence of wing aerodynamics was not further investigated.

Figure 6 presents the damping ratio results for the three main structural modes for different wing aerodynamics models, while Fig.7 compares combinations of wing and rotor aerodynamics of different fidelity levels. The beamwise mode results in Fig. 6a, characterized by out-of-plane wing bending, demonstrate the improvement in damping prediction obtained by improving the aerodynamic model's fidelity (greater damping, as shown later in Fig. 8a). The baseline model predicts an unrealistically low whirl flutter speed, contradicting both pre-test simulations [30] and experimental results [24], which never exhibited instability for the beamwise mode. While the DUST lifting line model predicts a moderately higher whirl flutter speed, the results clearly indicate that modeling the wing with at least the vortex lattice approach is necessary to capture the full aerodynamic effect. The surface panels approach yields results comparable to the vortex lattice model but incurs significantly higher computational costs. For the chordwise mode

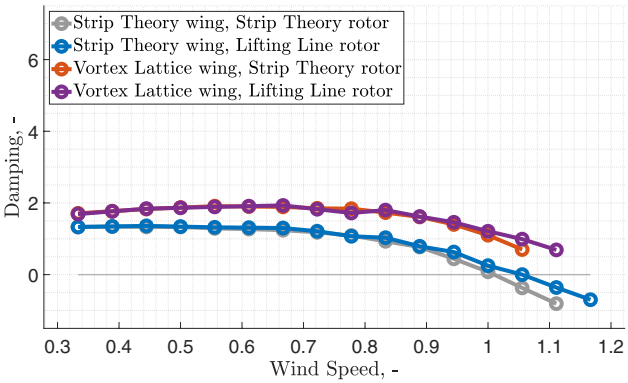

(a) Beamwise mode damping.

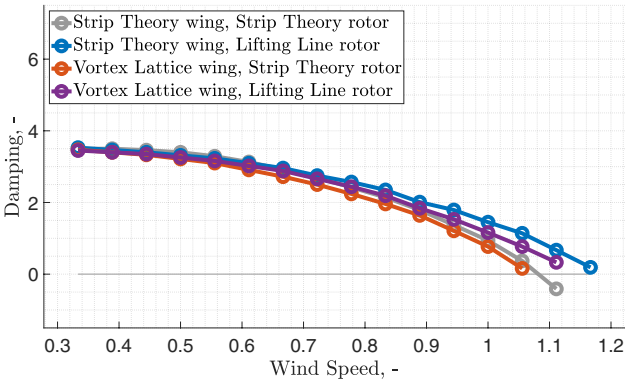

(b) Chordwise mode damping.

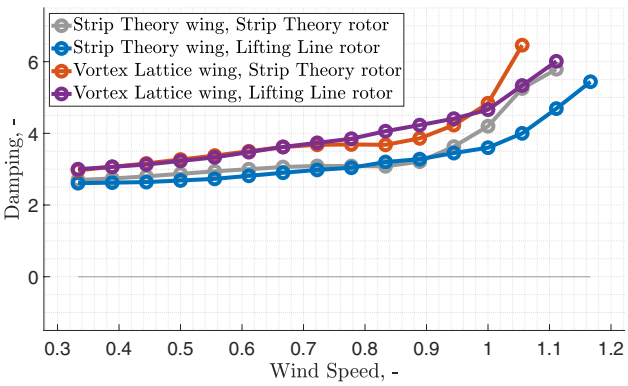

(c) Torsion mode damping.

Fig. 7 Analysis of aerodynamic contributions to structural mode damping

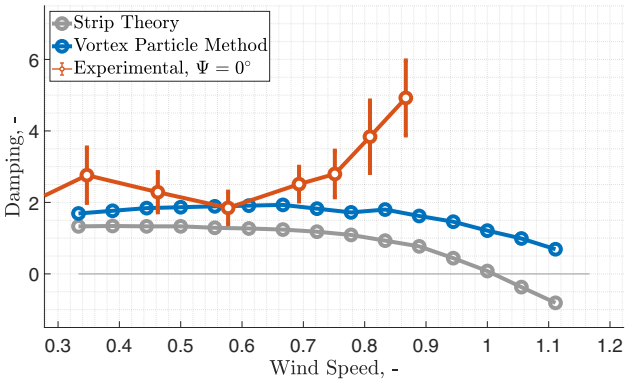

(a) Beamwise mode damping.

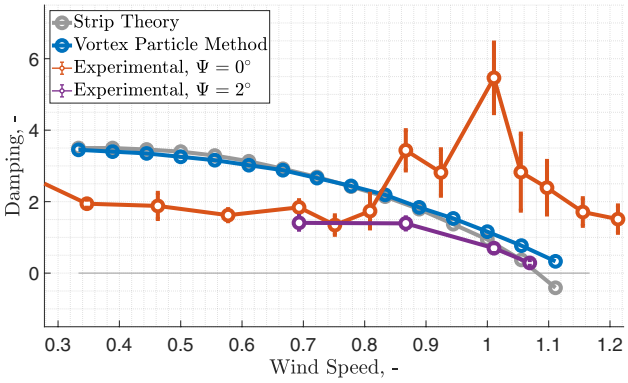

(b) Chordwise mode damping.

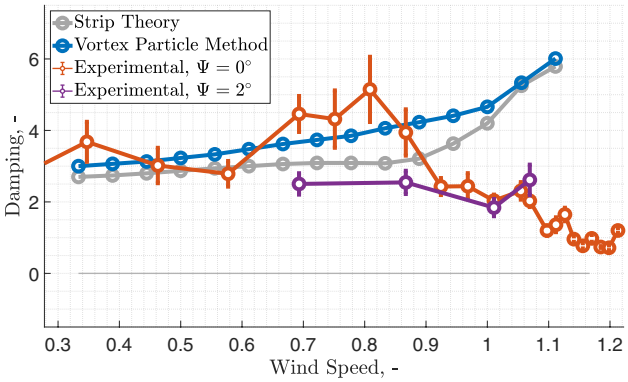

(c) Torsion mode damping.

Fig. 8 Structural modes damping: strip theory for wing and rotor, and vortex lattice for wing and lifting line for rotor, compared with experimental results with and without tilting

in Fig. 6b, all three DUST aerodynamic models produce results in close agreement, while MBDyn's strip theory model predicts slightly lower whirl flutter speeds.

The torsion mode in Fig. 6c shows a distinct separation between the lifting line approach and the higher-fidelity models, with MBDyn's strip theory results positioned intermediately between these extremes. The comparative analysis demonstrates that the vortex lattice model provides sufficient fidelity to capture the essential aerodynamic effects of the vortex particle method. However, it should be noted that when implementing the vortex lattice model for wing aerodynamics, simulations tend to encounter numerical divergence at lower speeds compared to both surface panels and lifting line implementations. Nevertheless, the

vortex lattice model is deemed a sufficient trade-off between numerical cost and accuracy.

A critical step in leveraging the mid-fidelity aerodynamic models is to understand the source of the increased damping observed in Fig. 6. To isolate individual aerodynamic contributions, a systematic analysis was conducted comparing four distinct modeling configurations as shown in Table 1.

The analysis examines the individual and combined effects of representing wing and rotor aerodynamics using either MBDyn's strip theory or DUST's VPM methodology. This approach enables the identification of which aerodynamic component, wing, rotor, or both, contributes most significantly to the damping predictions observed in the mid-fidelity models.

Figure 7 presents the comparative results of the four aerodynamic modeling configurations, revealing distinct patterns of influence for each structural mode. For the beamwise bending mode (Fig. 7a), the significant increase in damping is observed only when the wing is represented using DUST, with Case 2 closely tracking the results of the full DUST model (Case 4). This suggests that the enhanced damping prediction for this out-of-plane mode is primarily attributable to the higher-fidelity aerodynamic representation of the wing rather than the rotor, as already pointed out in [24].

The chordwise bending mode analysis (Fig. 7b) reveals a more complex interaction between aerodynamic components. In principle, wing aerodynamics should only marginally affect this mode. The most significant aerodynamic contribution is expected from the essentially uniform perturbation of rotor blade angle of attack caused by the oscillation of the wing tip along the rotor's axis, complemented by some nacelle yawing accompanied by disk tilting and precession caused by gyroscopic and aerodynamic loads. The full DUST model (Case 4) predicts damping levels that fall between Cases 2 and 3, suggesting that the observed chordwise mode damping of the mid-fidelity model, compared to the low-fidelity one, results from contrasting influences: a less destabilizing effect from the DUST-modeled rotor combined with a less stabilizing effect from the DUST-modeled wing. The hybrid approaches (Cases 2 and 3) would either over- or under-predict stability margins for this critical mode, which typically first encounters whirl flutter when considering DUST results.

Just like the beamwise bending mode, for the torsional mode (Fig. 7c), Case 2 tracks closely with the full DUST model at lower velocities but tends to deviate as speed increases. Case 3 substantially underestimates damping, even more severely than the baseline MBDyn model (Case 1).

Table 1 Tested aerodynamic modeling configurations

	Rotor	
Wing	MBDyn (strip theory)	DUST (lifting line)
MBDyn (strip theory)	Case 1	Case 2
DUST (vortex lattice)	Case 3	Case 4

The comprehensive analysis across all three structural modes reveals distinct patterns of aerodynamic influence on whirl flutter stability. The out-of-plane modes (beamwise and torsional) are primarily affected by the modeling of the wing using DUST, with the VPM approach capturing critical aerodynamic behaviors that the strip theory fails to represent. For the chordwise mode, both wing and rotor aerodynamic representations significantly influence stability predictions, with the combined effects determining the overall damping behavior. The full DUST model ultimately appears to provide the most accurate stability assessment, according to experimental results shown later in Fig. 8, especially for determining operational limitations defined by the critical chordwise mode.

The last step of this analysis involves comparing the simulation results with experimental data to gauge the impact of the enhanced modeling approaches. The experimental results were obtained from the ATTILA wind tunnel test campaign conducted at the DNW Large Low-speed Facility in late 2023 [24]. Flutter characteristics in airplane mode were identified from the free response data obtained after dwell excitations of each mode derived through the command of the swashplate mechanism. The data processing employed Leonardo's internally developed methods based on the Matrix Pencil algorithm for extracting frequency and damping parameters from the wing root and pylon balance strain gauge measurements. In general, both the experimental and numerical identification techniques are quite similar. As discussed in Sect. 1, a critical observation from the experimental campaign was the significant sensitivity of the chordwise mode damping to rotor disk tilting with respect to the mast. The experimental data revealed a considerable difference in the modes' damping trends between the untilted and tilted configurations, whereas frequencies were essentially unaffected. Due to this sensitivity, the experimental results are presented for both the untilted (zero gimbal angle) and tilted (2 deg gimbal angle) configurations to provide a comprehensive comparison with the numerical models.

Figure 8 compares the baseline MBDyn model, the DUST-enhanced model, and experimental measurements for all three structural modes in both configurations. The experimental results are shown with error bars representing 2σ variation in the damping identified by Leonardo from the free response to swashplate sinusoidal dwell excitations using the Bootstrap methodology [49]. Concerning the beamwise mode, no tests were conducted with a non-zero gimbal angle. The examination of the experimental results reveals a clear distinction between the tilted and untilted configurations. In the tilted configuration, the

damping trends follow relatively smooth and predictable paths, whereas the untilted configuration exhibits considerably more erratic behavior with pronounced oscillations and sudden variations across the wind speed range.

The comparison reveals limited correlation between numerical predictions and experimental results across all modes. Most significantly, neither the MBDyn nor DUST models exhibit any sensitivity to gimbal angle, producing identical damping trends for both tilted and untilted configurations. This fundamental discrepancy indicates that the observed experimental behavior cannot be captured through aerodynamic enhancements alone and thus suggests it is of a different nature. The pronounced sensitivity to gimbal angle observed in the experimental data, particularly the erratic damping behavior at zero gimbal angle, strongly suggests the presence of nonlinear mechanical effects not represented in the current models. As noted in [26], this behavior likely stems from structural nonlinearities in the rotor hub components, where friction and stiction phenomena may significantly influence the system dynamics at zero gimbal angle. Following these observations, the next phase of this investigation focuses on incorporating friction effects into the numerical models.

4 Friction

4.1 Motivation for friction analysis

The experimental observations from the ATTILA wind tunnel campaign and subsequent structural examination revealed several indicators pointing to friction as a potential source of the unexpected gimbal-angle-dependent behavior.

First, during both ground vibration testing and wind tunnel testing, nonlinearities in the system response were observed. These nonlinearities were particularly evident in the sensitivity of the chordwise mode damping to gimbal angle, which showed significantly different damping characteristics between tilted and untilted configurations, a phenomenon not predicted by the baseline numerical models, and also by the mid-fidelity analysis.

Second, post-test examination revealed wear patterns in the blade pitch encoder mechanism, as shown in [28], providing physical evidence of unanticipated friction interactions during testing. Additionally, observations during the test campaign suggested the presence of friction effects in other mechanical joints of the gimbal assembly.

Third, and most significantly, the experimental data demonstrated that the anomalous damping behavior was observed primarily in the untilted configuration, a condition where the control chain joints intrinsically experience minimal relative motion. Under such conditions, friction, and particularly stiction, could exert a dominant influence on the system dynamics. When the rotor disk was tilted about the gimbal joint, primarily by acting on the cyclic pitch, the damping trends exhibited an instantaneous transition to more predictable behavior, as evident in Fig. 8. This drastic change in dynamic characteristics with the presence of a non-zero gimbal angle strongly suggests that friction-induced locking in the hub components may be responsible for the phenomena observed in the experiments.

These observations collectively indicate that friction effects, particularly in the pitch encoders and gimbal assembly, warrant detailed investigation to understand their role in the experimentally observed whirl flutter characteristics.

4.2 Friction modeling approach

The accurate characterization of friction generally requires extensive experimental campaigns with specialized measurements necessary to precisely define and model friction parameters in each specific joint. Since such a comprehensive characterization was not feasible within the scope of this work, a different approach was adopted. Rather than pursuing an exact test-to-code correlation, this investigation focuses on understanding the qualitative effects of friction on the system's dynamic behavior and determining whether friction could explain the observed experimental phenomena.

To capture the most probable effects of friction, a stochastic approach was implemented using uncertainty quantification techniques. This methodology treats friction parameters as random variables with defined probability distributions, allowing exploration of how friction influences system stability across a realistic parameter space. By propagating these uncertain parameters through the model, the analysis provides insight into the sensitivity of whirl flutter characteristics to friction effects.

Friction models can be broadly categorized into static and dynamic formulations. Static friction models, such as the classical Coulomb model, represent steady-state behavior but cannot capture time-dependent phenomena. Dynamic friction models, conversely, account for effects such as pre-sliding behavior, hysteresis, and the Stribeck effect.

The two friction models offered by MBDyn were considered in this investigation. The discrete Coulomb model,

$$F_f = -F_n \left(\mu \operatorname{sgn}(\dot{x}) + \sigma_2 \dot{x}\right), \tag{1}$$

with transition to stiction when $|\dot{x}|$ falls below a given threshold, and transition to sliding when the tangential force component overcomes the static limit $|F_t| > \mu F_n$, provides a computationally efficient static representation with viscous damping and provisions for stick–slip transitions. The

LuGre model represents a more sophisticated dynamic formulation, capturing the complete range of friction phenomena through its representation of asperity deformation and velocity-dependent effects [26]. Since this study focuses on qualitative probabilistic analysis, the additional accuracy of the LuGre model is not required. Furthermore, the discrete Coulomb model reduces the number of parameters compared to the LuGre model, thereby decreasing the sample points needed for statistically meaningful uncertainty analysis. MBDyn implements friction modeling in a limited set of joint types. The two joints relevant to this study are revolute hinges, which constrain all degrees of freedom except rotation about a single axis, and spherical hinges, which allow all three rotational degrees of freedom. To incorporate friction effects in the testbed's multibody model, the original formulation must be modified to represent critical connection points using these joint types.

The uncertainty quantification framework, implemented through DAKOTA [50], controls multiple MBDyn simulations across the parameter space. This approach enables statistical characterization of friction's influence on modal damping and frequency, as well as the *duty cycle*, a metric representing the fraction of time spent in the stick condition during the free response. This comprehensive analysis provides robust insights into how friction can affect both the stability characteristics and the stick–slip behavior of the system.

4.3 Pitch encoder friction analysis

The ATTILA testbed's blade attachment, shown in Fig. 3, consists of pairs of bearings that connect each blade to the yoke. The inner bearing (point 1 in Fig. 3), positioned at the blade root, constrains flapwise and chordwise displacements, while the outer bearing (point 2 in Fig. 3), located further outboard along the yoke, constrains all translational degrees of freedom. Together, these bearings allow only pitch rotation about the blade's feathering axis, with the angle measured by dedicated pitch encoders positioned between the bearings (point 3 in Fig. 3).

During the wind tunnel testing campaign, adhesion was observed between components of the pitch encoder mechanism. This effect, not anticipated in the original design and possibly caused by improper material selection, resulted in sliding friction between two aluminum surfaces. Post-test examination confirmed wear patterns on the encoder components, providing physical evidence of friction development during operation.

To incorporate these friction effects into the numerical model while maintaining the original load paths, a modification of the existing MBDyn joint formulation was required. The original implementation utilized for both bearings a *total joint*, an element that allows for arbitrary constraining of specific components of the relative position and orientation between two parts. The total joint does not enable friction modeling, so a different approach was required. The outer bearing remains unchanged, while the inner bearing is split into two parts, connected by a revolute joint, an element capable of incorporating friction models.

The standard MBDyn friction implementation calculates the normal force based on the constraint reactions in the joint, which in this case would coincide with the inner-bearing constraint reactions. Since the encoder mechanism was designed to operate unloaded and was placed close to the outer bearing, it certainly cannot sustain the magnitude of forces typically carried by the inner bearing. To address this limitation, a modified version of the MBDyn revolute hinge friction model was implemented. Instead of using the constraint reactions, this model employs a user-defined constant preload as the normal force for friction calculations. This approach better represents the physical situation where the encoder surfaces experience contact pressure from installation tolerances or assembly preload, rather than from the structural loads transmitted through the bearing.

To implement the uncertainty propagation analysis for the pitch encoder friction, a careful parameterization of the Coulomb viscous model was necessary. This model requires five parameters to fully characterize friction behavior.

In the modified Coulomb model implemented in MBDyn, it was observed that changing the radius, preload, or friction coefficient had equivalent effects on the resulting static friction moments. This means that for uncertainty quantification purposes, these three parameters can be effectively represented by a single variable, significantly reducing the dimensionality of the parameter space and the number of simulations required for statistically meaningful results.

With this simplification, the uncertainty analysis focused on two primary variables:

- The preload P range was selected to represent realistic contact scenarios between the encoder surfaces. The lower bound of 10 N represents a minimal contact pressure that could develop due to minor misalignment or vibration, while the upper bound of 100 N represents a more substantial contact pressure that might result from assembly preload or thermal expansion. This range provides a comprehensive exploration of potential friction conditions without extending into physically unrealistic territories.
- The viscous damping coefficient σ_2 affects energy dissipation during the slip phase. A relatively narrow range was selected. This parameter typically has less impact on overall system behavior than the static friction

parameters, but it can influence the energy dissipation characteristics during slip conditions.

By treating these parameters as uncertain variables with defined distributions, the uncertainty propagation analysis systematically explores the parameter space to determine how friction affects the stability characteristics of the system across different operating conditions and gimbal angles.

Figure 9 shows the results from the uncertainty propagation analysis for three tilt angles compared to the reference damping trends of the frictionless system. The shaded regions represent one standard deviation above and below the mean value, capturing approximately 68% of the simulation results. The analysis reveals clear sensitivity to the tilt of the rotor disk across all modes, though with varying patterns.

For the beamwise mode (Fig. 9a), damping trends rapidly revert to the frictionless system behavior as soon as tilt is induced through the cyclic pitch control. The untilted configuration exhibits higher damping, particularly at low to mid airspeeds, where the duty cycle parameter approaches 100%, indicating the system remains predominantly in the stick condition. This locked state effectively changes the overall stiffness of the system, causing the elevated damping levels. In contrast, the torsion mode (Fig. 9c) presents an unexpected pattern where the untilted configuration most closely resembles the reference frictionless case, while the tilted configurations show increased damping. The chordwise mode (Fig. 9b) presents a more gradual variation in damping trends with changes in rotor tilt angle. However, contrary to experimental observations, the numerical results predict higher damping for all configurations compared to the frictionless system. The addition of friction in the encoders has a stabilizing effect on the chordwise mode, which directly contradicts the experimental findings where the chordwise mode became considerably less stable with applied tilt, and ultimately became the critical flutter mode.

This tilt sensitivity is primarily attributed to the effects of stiction, summarized by the duty cycle parameter, which represents the percentage of time spent in the stick condition during the free response. In the untilted configuration, small oscillations of the blades around the feathering axis struggle to overcome stiction, resulting in duty cycle values approaching 100% at lower airspeeds, especially for higher friction configurations. As tilt is applied, the cyclic pitch motion induced by the gimbal angle generates sufficient moments to consistently break free from stiction, significantly reducing the duty cycle.

While the pitch encoder friction model successfully captures some tilt-dependent behavior, it fails to reproduce the experimental observation that the chordwise mode becomes less stable with applied tilt. This fundamental discrepancy suggests that encoder friction alone cannot explain the observed experimental phenomena. It is important to note

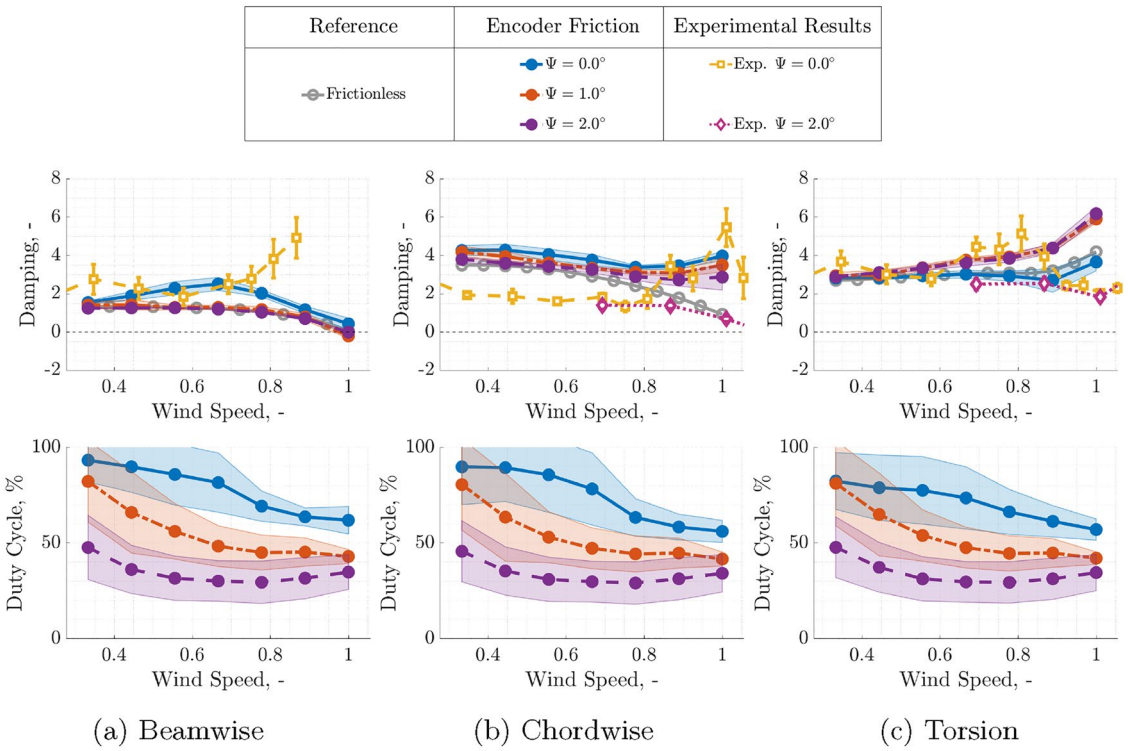

Fig. 9 Effect of pitch encoder friction on structural mode damping

that the wear patterns observed on the encoder components provide concrete evidence that friction was indeed present in these assemblies during testing, and likely evolved (increased) with usage. However, the proposed model may either overestimate the magnitude of this friction or the experimentally observed behavior may result from complex interactions between encoder friction and friction in other joints of the system. The isolated encoder friction effects may be necessary but insufficient to fully capture the observed dynamics, suggesting that a more comprehensive friction model incorporating multiple joints might be required, as discussed in the next Section.

4.4 Gimbal joint friction analysis

The gimbal joint assembly, shown in Fig. 4, represents one of the most critical mechanical interfaces in the tiltrotor testbed. This complex assembly consists of a central spherical bearing and three compass mechanisms arranged radially around the mast.

The spherical bearing (point 1 in Fig. 4), positioned at the interface between the mast and the rotor hub, permits the rotation about all three axes while constraining translational motion and transmitting forces between the rotor and the shaft. This component consists of two steel plates with a spherical recess that rotate around a spherical element made of bronze, with lubrication. Meanwhile, the three compass mechanisms (one highlighted by point 2 in Fig. 4) serve a dual purpose: they transmit rotational motion and carry torque from the mast to the rotor disk around the shaft axis while accommodating the tilting of the rotor disk by allowing rotation about the remaining two axes perpendicular to the shaft. Each compass consists of two aluminum arms connected by a spherical joint. The lower arm attaches to the mast through a revolute hinge, while the upper arm similarly connects to the upper plate of the hub assembly. The revolute hinges rotate around steel pins with bronze bushings and are lubricated to minimize friction, while the spherical bearings connecting the two arms are standard commercial components.

Implementing friction in the gimbal assembly required significant modifications to the original MBDyn model. The initial, frictionless implementation used MBDyn's gimbal rotation joint, a specialized element that approximates an ideal tiltrotor gimbal. However, since friction depends on the constraint reactions, the actual load paths need to be reproduced in detail.

The spherical joint at the center of the gimbal assembly was readily implemented using MBDyn's spherical hinge element, enhanced with friction support capabilities based on an original formulation that will be the subject of a forthcoming publication. The compass mechanisms presented a more complex challenge. In the physical testbed, three compass assemblies are used to ensure robust torque transmission and balanced load distribution. However, from a kinematic perspective, a single compass would be sufficient to constrain the system, when modeled using rigid parts as in the present case. Implementing all three compasses in the numerical model creates redundant constraints that would lead to an ill-conditioned mathematical problem.

To overcome this challenge while maintaining physical fidelity, all three compasses were modeled using a constraint regularization strategy based on the Tikhonov method. This approach modifies the constraint equations through the introduction of a compliance coefficient, effectively transforming rigid constraints into stiff elastic connections. Mathematically, this can be interpreted as replacing an infinitely stiff constraint with a finite but very large stiffness value. The regularization compliance, placed over the compass spherical hinges, was carefully tuned to the lowest possible value that maintained numerical stability while minimizing constraint violations. This approach allowed for the realistic representation of the complete compass assembly, including the potential for different friction characteristics in each compass, without creating an over-constrained system that would be numerically intractable.

Friction can be represented in all of the joints of the gimbal assembly. Testing friction representation in the compasses required unrealistically high levels of friction to obtain tangible differences in the system's behavior, likely owing to the small reaction forces transmitted by the joints. Conversely, representing friction in the gimbal's spherical hinge showed interesting results with realistic levels of friction. Although the actual amount of friction in the gimbal assembly is completely unknown, this part of the analysis aims at exploring what its effects would be concerning the tilting of the rotor and, in particular, whether friction-induced blocking of the tilting motion can affect the system dynamics.

The approach employed models friction only within the gimbal spherical hinge, using a Coulomb friction formulation in which the normal force corresponds to the reaction constraint inside the gimbal joint. This methodology captures a realistic scenario, since the spherical hinge carries the full load transmitted between the mast and the rotor assembly, providing a physically meaningful basis for friction calculations.

Only the normal component of the reaction (a scalar) is taken as the Lagrange multiplier of the spherical joint; both the tangent friction force and the friction-induced moment are then computed as functions of the friction coefficient and of the normal reaction force. As a result, the total force exchanged between the two bodies through the joint includes both the normal reaction and the tangential friction

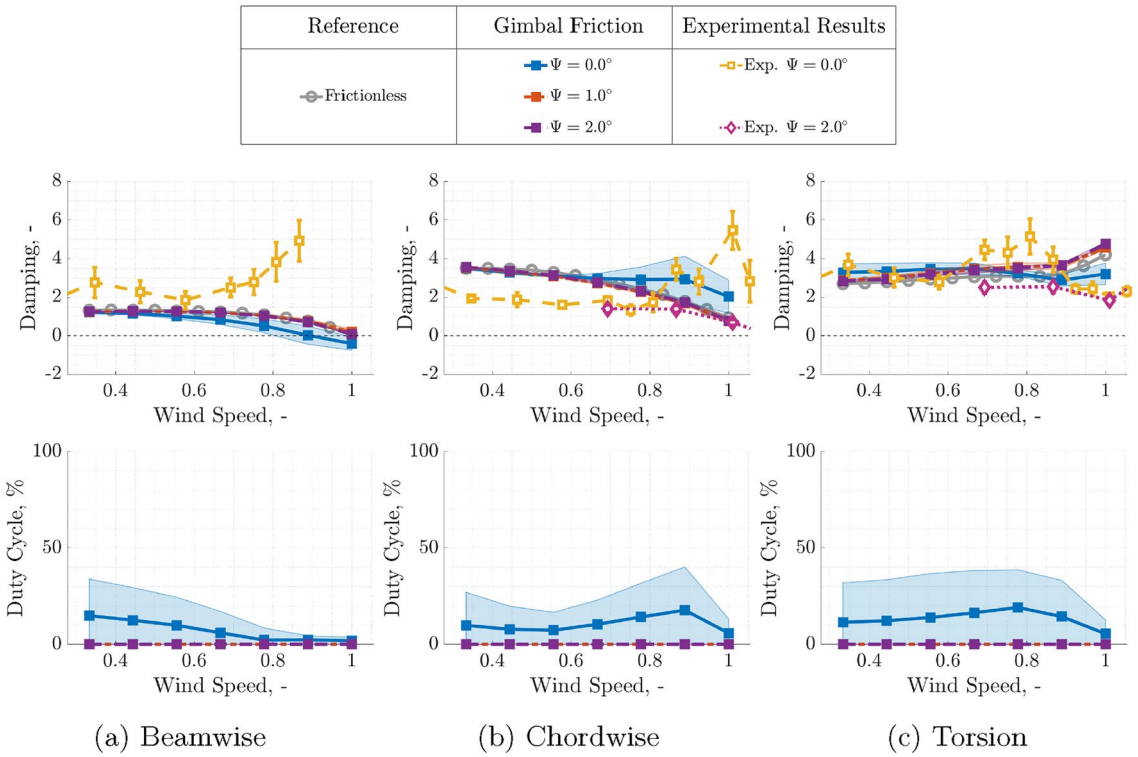

Fig. 10 Effect of gimbal spherical friction on structural mode damping

components. This approach differs from that implemented in many commercial multibody solvers, which account for friction solely through the friction-induced moment, computed as a function of the friction coefficient and of the overall force resultant, potentially overestimating it but, at the same time, significantly simplifying the joint formulation.

For example, in ANSYS Mechanical Application revolute joints[3] the frictional tangential stress is assumed to be uniformly distributed around the joint, so that the resulting force cancels out and only the net friction torque is considered; the friction force is neither computed nor reported. In ADAMS,[4] the reaction force is not considered, and only the reaction moment is. In COMSOL,[5] since joints are abstractions, there is no definition of the normal reaction force to which the friction force should be proportional. Multiple methods are available to compute the normal force for a given joint, and the user must select the most appropriate one.

In the proposed formulation, the point of contact is identified using the direction of the normal reaction force. When the joint is sticking, the friction-induced force prevents relative displacement at the point of contact. No attempt is made to model the so-called moment of rotational friction [51], which acts about an axis aligned with the normal reaction force.

For the uncertainty quantification analysis, the friction parameters were defined as shown in Table 3. The spherical hinge's actual radius was held constant, while the friction coefficient varied between reasonable bounds for lubricated bronze-steel interfaces. The lower bound represents well-lubricated conditions, while the upper bound accounts for potential degradation of lubrication effectiveness during operation or other unexpected problems that may affect the free tilting of the rotor disk.

Figure 10 presents the results from the uncertainty propagation analysis for the gimbal spherical hinge friction. The analysis reveals distinct patterns that differ significantly from the pitch encoder friction results of Fig. 9. The time spent in the stick condition is considerably lower compared to the encoder friction case. Most notably, as soon as tilt is applied to the rotor disk, the effects of friction nearly disappear since stiction no longer occurs in the gimbal joint.

For the beamwise mode (Fig. 10a), the untilted configuration shows markedly reduced damping compared to both the tilted configurations and the reference frictionless

[3] https://ansyshelp.ansys.com/public/account/secured?returnurl=////Views/Secured/corp/v242/en/wb_sim/ds_joint_friction_joint_types.html, last accessed December 2025.

[4] https://nexus.hexagon.com/documentationcenter/en-US/bundle/simd_2023.1_r2022/page/simd_2023.1_r2022/simd4catia_motion_guide/ref_motion_guidev2/TOC.Friction.Results.xhtml, last accessed December 2025.

[5] https://doc.comsol.com/5.5/doc/com.comsol.help.mbd/mbd_ug_theory.4.20.html, last accessed December 2025.

system. This behavior indicates that friction, most notably stiction, in the gimbal joint has a destabilizing effect on the beamwise mode when the rotor operates without tilt. The locking of the gimbal motion, as evident from the duty cycle parameter, restricts the system's ability to naturally respond to the loads developed, leading to a considerably less stable beamwise mode. It is important to note that beamwise damping requires representation through the VPM to be accurately captured, but even so, the behavior differs considerably from the experimentally identified trends. The chordwise mode (Fig. 10b) demonstrates the most dramatic sensitivity to gimbal angle, being characterized by considerably higher damping in the untilted configuration at high airspeeds. Conversely, in the tilted configuration, the damping trends revert to the original frictionless system behavior. The torsion mode (Fig. 10c) presents an intermediate response, with the untilted configuration showing moderately reduced damping at higher speeds compared to the tilted cases, though the effect is less pronounced than for the chordwise mode.

The mechanism underlying these results can be understood through the role of the gimbal joint in tiltrotor dynamics. Under normal operating conditions, the gimbal allows the rotor disk to freely articulate, providing a degree of isolation between rotor forces and the supporting structure. When friction in the gimbal joint becomes significant, particularly under low-motion conditions characteristic of the untilted configuration, stiction can effectively lock the gimbal degrees of freedom. This locking transforms the rotor mounting from a flexible, articulated system to a rigid connection, fundamentally altering the load paths and dynamic response characteristics of the entire assembly. The transition from locked to unlocked gimbal behavior with applied tilt occurs because the cyclic pitch motion required to maintain the gimbal angle generates sufficient moments to overcome static friction, restoring the intended articulated behavior of the gimbal joint.

4.5 Combined friction effects

To investigate the potential synergistic effects of friction across multiple joints, a preliminary analysis was conducted, incorporating both pitch encoder and gimbal spherical hinge friction simultaneously. This combined approach recognizes that, in the physical system, multiple sources of friction likely coexist and may interact to produce the observed experimental behavior. The gimbal joint and blade pitching mechanisms are kinematically coupled through the flexible control chain, meaning their motions are not independent. For instance, when cyclic commands are held constant, the tilting of the rotor disk necessarily induces blade pitching motion to maintain the prescribed control inputs.

Table 2 Encoder hinge friction parameters for uncertainty propagation analysis

Parameter		Value/range
r	mm	10 (fixed)
μ		1.0 (fixed)
P	N	10–100
σ_2	$\mathrm{N{\cdot}s{\cdot}m^{-1}}$	0.0–0.2

Table 3 Gimbal spherical hinge friction parameters for uncertainty propagation analysis

Parameter		Value/range
r	mm	25 (fixed)
μ		5×10^{-3}–2.5×10^{-1}
σ_2	$\mathrm{N{\cdot}s{\cdot}m^{-1}}$	0.0–0.1

Table 4 Combined friction analysis parameters

Parameter		Encoder	Gimbal
r	mm	10 (fixed)	25 (fixed)
μ		1.0 (fixed)	5×10^{-3}–2.5×10^{-1}
P	N	10–100	Not applicable
σ_2	$\mathrm{N{\cdot}s{\cdot}m^{-1}}$	0.0–0.2 (shared)	

This coupling creates a scenario where friction in one component can influence the behavior of another. Specifically, stiction in the pitch encoders could restrict blade motion, which in turn affects the relative motion between the mast and rotor hub, potentially facilitating the development of stiction in the gimbal joint. Furthermore, the physical evidence of wear patterns observed when the encoder components were disassembled between test runs confirms that friction was indeed present in these assemblies during the test campaign. While the magnitude and precise characteristics of this friction remain uncertain, its presence cannot be dismissed when attempting to understand the system's overall dynamic behavior.

For the uncertainty quantification analysis of the combined friction effects, the same parameter ranges established for the individual friction studies were employed (Table 4). The pitch encoder friction parameters remained consistent with Table 2, while the gimbal spherical hinge parameters followed those defined in Table 3. However, a key simplification was implemented to maintain computational feasibility: for both joints the viscous damping coefficient (σ_2) was constrained to have identical values throughout each simulation. This constraint was necessary because introducing an additional independent variable would exponentially increase the required sample size for statistically meaningful results. In this manner, the parameter space dimensionality was maintained at a manageable level while still capturing the essential friction interactions.

Figure 11 presents the results of the combined friction analysis, which reveals distinctly different system behavior,

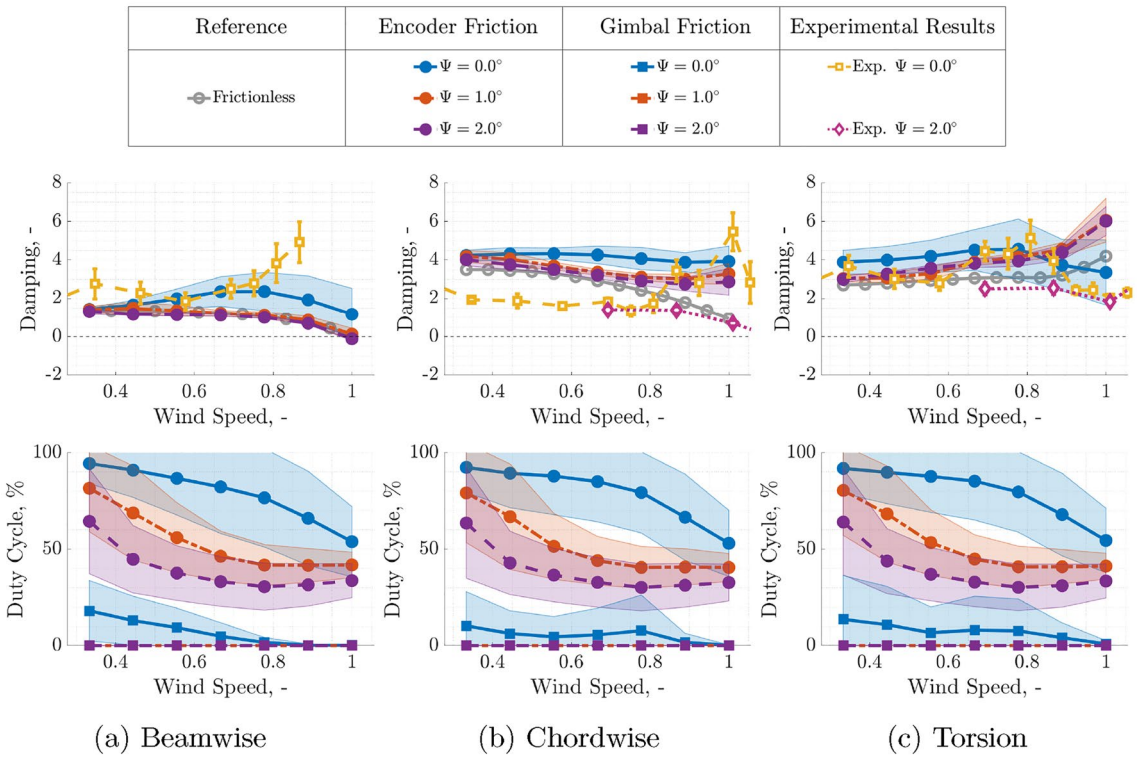

Fig. 11 Effect of combined gimbal spherical friction and encoder friction on structural mode damping

particularly in the untilted configuration. As observed in the gimbal-only friction case (Fig. 10), the application of tilt to the rotor disk effectively eliminates most friction effects, with the exception of the torsional mode. This means that in the combined friction case, the tilted configuration behavior closely resembles that observed in the encoder-only friction analysis (Fig. 9).

The beamwise mode (Fig. 11a) exhibits a particularly interesting behavior in the untilted configuration. Rather than showing a simple superposition of the individual encoder and gimbal friction effects, the results demonstrate a complex interaction between the two friction sources. This interaction leads to a considerably more damped beamwise mode compared to either individual case, though the predicted behavior still differs significantly from the experimental observations. The chordwise (Fig. 11b) and torsional mode (Fig. 11c) display behavior that more closely resembles a combination of the two separate friction cases. The untilted configuration shows characteristics influenced by both friction sources, while the tilted configurations primarily reflect the encoder friction effects due to the elimination of gimbal stiction when rotor tilt is applied.

5 Conclusions

The most important results of this investigation are summarized as follows:

1. **Mid-fidelity aerodynamic modeling:** The combination of the vortex-particle free-wake model and the vortex-lattice representation of the wing in DUST generally yields a more accurate description of the physics involved in the aerodynamic contribution to equivalent damping for out-of-plane modes compared with a strip-theory-based approach. The vortex-lattice method offers an optimal balance between accuracy and computational efficiency. However, neither the baseline MBDyn model nor the DUST-enhanced model exhibits significant sensitivity to rotor disk tilt.
2. **Friction effects in mechanical joints:** The stochastic friction analysis shows that mechanical friction—particularly in the gimbal spherical hinge—can produce measurably distinct dynamic responses between tilted and untilted configurations. This occurs through stick–slip mechanisms that fundamentally modify the equivalent system stiffness. In particular, stiction-induced locking emerges as a plausible mechanism underlying the observed experimental behavior.
3. **Combined friction effects:** The simultaneous presence of friction in both pitch encoders and gimbal

components leads to a response that differs from the simple superposition of individual effects. This suggests that multiple friction sources may interact synergistically in the physical system.

Overall, the use of multibody analysis coupled with mid-fidelity aerodynamics, and its ability to represent relatively sophisticated nonlinear behaviors, enabled the verification of plausible explanations for experimental evidence that would remain inaccessible through conventional aeroelastic simulation tools.

The results further underscore the usefulness to account for nonlinear joint behaviors when interpreting experimental evidence, as friction can obscure or amplify dynamic phenomena. The identified mechanisms offer guidance toward more accurate modeling strategies that better reconcile numerical predictions with observations.

Acknowledgements The authors acknowledge the contribution of Dr. Alessandro Cocco to the implementation of DUST and of the initial development of the MBDyn and DUST numerical models. The ATTILA project has received funding from Clean Sky 2 Joint Undertaking (JU) under grant agreement No. 863418. The JU receives support from the European Union's Horizon 2020 research and innovation programme and the Clean Sky 2 JU members other than the Union.

Author contributions PdV, GC, MM, and PM wrote the main manuscript text; PdV and GC developed the numerical models, performed the calculations, and analyzed the results; MM developed the friction-related part of the software; FF, MF, and SvH compared the results with experiments; all authors equally contributed to the conceptual part and reviewed the manuscript.

Funding Open access funding provided by Politecnico di Milano within the CRUI-CARE Agreement.

Data availability Data must be requested to the ATTILA Consortium. Contact the Corresponding Author for further information.

Declarations

Conflict of interest The fourth author, Pierangelo Masarati, is an Associate Editor of the CEAS Aeronautical Journal, but was not involved in the peer review process at any stage. All other authors have no conflict of interest to declare that are relevant to the content of this article.

References

1. Popelka, D., Sheffler, M., Bilger, J.: Correlation of test and analysis for the 1/5-scale V-22 aeroelastic model. J. Am. Helicopter Soc. **32**(2), 21–33 (1987). https://doi.org/10.4050/JAHS.32.21
2. Settle, T.B., Kidd, D.L.: Evolution and test history of the V-22 02-scale aeroelastic model. J. Am. Helicopter Soc. **37**(1), 31–45 (1992). https://doi.org/10.4050/JAHS.37.31
3. Piatak, D.J., Kvaternik, R.G., Nixon, M.W., Langston, C.W., Singleton, J.D., Bennett, R.L., Brown, R.K.: A wind-tunnel parametric investigation of tiltrotor whirl-flutter stability boundaries. In: American Helicopter Society 57th Annual Forum, Washington, DC (2001)
4. Acree, C.W.: Effects of rotor design variation on tiltrotor whirl-mode stability. In: Tiltrotor/Runway Independent Aircraft Technology and Applications Specialists' Meeting of the American Helicopter Society, Arlington, TX, USA (2001)
5. Masarati, P., Piatak, D.J., Quaranta, G., Singleton, J.D., Shen, J.: Soft-inplane tiltrotor aeromechanics investigation using two comprehensive multibody solvers. J. Am. Helicopter Soc. **53**(2), 179–192 (2008). https://doi.org/10.4050/JAHS.53.179
6. Kang, H., Shen, J., Kreshock, A.R.: Validation of comprehensive analysis for tiltrotor whirl flutter predictions. J. Aircr. **54**(4), 1566–1570 (2017). https://doi.org/10.2514/1.C034272
7. Kreshock, A.R., Thornburgh, R.P., Yeo, H.: Comparison of comprehensive analyses predicting aeroelastic stability of the wing and rotor aeroelastic test system. In: AHS 74th Annual Forum, Phoenix, AZ, USA (2018)
8. Nannoni, F., Giancamilli, G., Cicalè, M.: ERICA: the European Advanced Tiltrotor. In: 27th European Rotorcraft Forum, Moscow, Russia, pp. 55–115 (2001)
9. Krüger, W.R.: Multibody analysis of whirl flutter dynamics on a tiltrotor wind tunnel model. In: International Forum on Aeroelasticity and Structural Dynamics, Seattle, Washington, USA (2009). Paper No. IFASD-2009-022
10. Krüger, W.R.: Multibody analysis of whirl flutter stability on a tiltrotor wind tunnel model. Proc. IMechE, Part K: J. Multi-body Dyn **230**(2), 121–133 (2016). https://doi.org/10.1177/1464419315582128
11. Cugnon, F., Eberhard, A.: Aeroelastic modeling of the hub and blade rotor system of the NICETRIP tilt-rotor aircraft using mecano FEM multibody solver, Gallarate, Italy, pp. 896–902 (2011). Paper no. 192
12. Kreshock, A.R., Acree, C.W., Kang, H., Yeo, H.: Development of a new aeroelastic tiltrotor wind tunnel testbed. In: AIAA Scitech 2019 Forum, San Diego, CA, USA (2019). https://doi.org/10.2514/6.2019-2133
13. Kreshock, A.R., Kang, H., Thornburgh, R., Yeo, H., Baggett, J., Shen, J.: Pretest flutter predictions of the upcoming aeroelastic tiltrotor wind tunnel test. In: Vertical Flight Society's 76th Annual Forum & Technology Display, Virtual (2020). https://doi.org/10.4050/F-0076-2020-16436
14. Yeo, H., Kang, H., Kreshock, A.R.: Modeling and analysis of proprotor whirl flutter. In: the Vertical Flight Society's 77th Annual Forum & Technology Display, Palm Beach, Florida, USA (2021). https://doi.org/10.4050/F-0077-2021-16771
15. Kreshock, A.R., Thornburgh, R., Wilbur, M.: Overview of the tiltrotor aeroelastic stability testbed. In: AIAA SCITECH 2022 Forum, San Diego, CA, USA & Virtual (2022). https://doi.org/10.2514/6.2022-0566
16. Kreshock, A.R., Thornburgh, R.P., Wilbur, M.L., Kang, H., Piatak, D.J., Sekula, M.K.: Initial whirl-flutter characterization of the tiltrotor aeroelastic stability testbed. In: Vertical Flight Society's 79th Annual Forum & Technology Display, West Palm

Beach, FL, USA (2023). https://doi.org/10.4050/F-0079-2023-18037
17. Yeo, H., Kang, H., Kreshock, A.R.: Unified modeling of the tiltrotor aeroelastic stability testbed for proprotor whirl flutter. J. Aircr. **60**(3), 857–869 (2023). https://doi.org/10.2514/1.C036950
18. Kreshock, A.R., Thornburgh, R.P., Kang, H., Yeo, H.: Experimental and analytical comparison of stiff and flexible rotor blades for tiltrotor whirl flutter stability. In: 50th European Rotorcraft Forum, Marseille, France (2024)
19. Gul, S., Datta, A.: Whirl flutter test of the Maryland tiltrotor rig: Prediction and validation. In: AIAA SciTech 2022 Forum, Dynamics Specialists Conference, San Diego, CA, USA (2022). https://doi.org/10.2514/6.2022-0927
20. Gul, S., Yeo, H.: Correlation of high-speed tiltrotor stability predictions with test data and parametric study. J. Aircr. **61**(4), 1283–1292 (2024). https://doi.org/10.2514/1.C037807
21. O'Brien, N., Delgado, X., Akinwale, A., Datta, A.: Fundamental understanding of hingeless hub proprotor stability. In: 50th European Rotorcraft Forum, Marseille, France (2024)
22. Riso, C.: Evaluation of whirl flutter prediction methods for a system with hardening or softening structural nonlinearities. J. Am Helicopter Soc. **70**(2), 1–1515 (2025). https://doi.org/10.4050/JAHS.70.022001
23. van't Hoff, S., van Vilsteren, J., Cocco, A., Masarati, P.: Design of a tiltrotor semi-span wind tunnel model for whirl flutter investigations. In: AIAA Scitech 2023 Forum, p. 1306 (2023). https://doi.org/10.2514/6.2023-1306
24. van 't Hoff, S., Fonte, F., De Vita, P., Cassoni, G., Masarati, P., Soal, K.: ATTILA tiltrotor whirl flutter code-to-test correlation. In: Vertical Flight Society 81st Annual Forum, Virginia Beach, VA, USA (2025). https://doi.org/10.4050/F-0081-2025-265
25. De Vita, P., Cassoni, G., Morandini, M., Masarati, P., Fonte, F., Favale, M., van 't Hoff, S.: Tiltrotor wind-tunnel model whirl flutter with mid-fidelity aerodynamics and mechanical friction. In: 51st European Rotorcraft Forum, Venice, Italy (2025). Paper 149
26. De Vita, P., Cassoni, G., Morandini, M., Masarati, P., Fonte, F., Favale, M., van 't Hoff, S.: Numerical whirl-flutter investigation of a multibody/vortex particle tiltrotor model with frictional components. In: Multibody 2025, Innsbruck, Austria (2025). Preprint (Version 1) available at Research Square, https://doi.org/10.21203/rs.3.rs-6511107/v1
27. Montaño-Oliveros, J., Fonte, F., van 't Hoff, S., Timmerman, B.: Whirl flutter analysis of a tiltrotor semi-span wind tunnel model for test results correlation. In: 49th European Rotorcraft Forum, Bückeburg, Germany (2023)
28. van 't Hoff, S., Fonte, F., Soal, K.I., Schneider, O., Kapteijn, K.: Whirl flutter testing of ATTILA tiltrotor testbed—initial results. In: Vertical Flight Society's 80th Annual Forum & Technology Display, Montréal, Québec, Canada (2024). https://doi.org/10.4050/F-0080-2024-1117
29. Cocco, A., Masarati, P., van 't Hoff, S., Timmerman, B.: Tiltrotor whirl flutter analysis in support of NGCTR aeroelastic wind tunnel model design. In: 47th European Rotorcraft Forum, Glasgow, UK (virtual) (2021)
30. Cocco, A., Masarati, P., van 't Hoff, S., Timmerman, B.: Numerical whirl-flutter analysis of a tiltrotor semi-span wind tunnel model. CEAS Aeronautical J. **13**(4), 923–938 (2022). https://doi.org/10.1007/s13272-022-00605-2
31. Masarati, P., Morandini, M., Mantegazza, P.: An efficient formulation for general-purpose multibody/multiphysics analysis. J. Computat. Nonlinear Dyn. **9**(4), 041001 (2014). https://doi.org/10.1115/1.4025628
32. Ghiringhelli, G.L., Masarati, P., Mantegazza, P., Nixon, M.W.: Multi-body analysis of a tiltrotor configuration. Nonlinear Dyn. **19**(4), 333–357 (1999). https://doi.org/10.1023/A:1008386219934
33. Ghiringhelli, G.L., Masarati, P., Mantegazza, P., Nixon, M.W.: Multi-body analysis of an active control for a tiltrotor. In: CEAS Intl. Forum on Aeroelasticity and Structural Dynamics 1999, Williamsburg, VA, pp. 149–158 (1999)
34. Masarati, P., Piatak, D.J., Singleton, J.D., Mantegazza, P.: An investigation of soft-inplane tiltrotor aeromechanics using two multibody analyses. In: American Helicopter Society 4th Decennial Specialists' Conference on Aeromechanics, Fisherman's Wharf, San Francisco, CA (2004)
35. Masarati, P., Piatak, D.J., Quaranta, G., Singleton, J.D.: Further results of soft-inplane tiltrotor aeromechanics investigation using two multibody analyses. In: American Helicopter Society 60th Annual Forum, Baltimore, MD (2004)
36. Masarati, P., Piatak, D.J., Quaranta, G., Singleton, J.D., Shen, J.: Soft-inplane tiltrotor aeromechanics investigation using two multibody analyses. In: 31st European Rotorcraft Forum, Firenze, Italy (2005)
37. Shen, J., Masarati, P., Piatak, D.J., Nixon, M.W., Singleton, J.D., Roget, B.: Modeling a stiff-inplane tiltrotor using two multibody analyses: a validation study. In: American Helicopter Society 64th Annual Forum, Montreal, Canada (2008)
38. Shen, J., Singleton, J.D., Piatak, D.J., Bauchau, O.A., Masarati, P.: Multibody dynamics simulation and experimental investigation of a model-scale tiltrotor. J. Am Helicopter Soc **61**(2), 1–11 (2016). https://doi.org/10.4050/JAHS.61.022010
39. Cocco, A., Savino, A., Masarati, P.: Flexible multibody model of a complete tiltrotor for aeroservoelastic analysis. In: ASME IDETC/CIE 2022, St. Louis, Missouri, USA (2022). https://doi.org/10.1115/DETC2022-88973
40. Cocco, A., Savino, A., Zanoni, A., Masarati, P.: Comprehensive simulation of a complete tiltrotor with pilot-in-the-loop for whirl-flutter stability analysis. In: 48th European Rotorcraft Forum, Winterthur, Switzerland (2022)
41. Cassoni, G., Cocco, A., Tamer, A., Zanoni, A., Masarati, P.: Rotorcraft stability analysis using Lyapunov characteristic exponents estimated from multibody dynamics. CEAS Aeronaut. J. **15**(3), 703–719 (2024). https://doi.org/10.1007/s13272-024-00724-y
42. Ghiringhelli, G.L., Masarati, P., Mantegazza, P.: A multi-body implementation of finite volume C^0 beams. AIAA J. **38**(1), 131–138 (2000). https://doi.org/10.2514/2.933
43. Bauchau, O.A., Betsch, P., Cardona, A., Gerstmayr, J., Jonker, B., Masarati, P., Sonneville, V.: Validation of flexible multibody dynamics beam formulations using benchmark problems. Multibody Sys.Dyn. **37**(1), 29–48 (2016). https://doi.org/10.1007/s11044-016-9514-y
44. Leishman, J.G.: Principles of Helicopter Aerodynamics, 2nd edn. Cambridge University Press, Cambridge, UK (2006)
45. Savino, A., Cocco, A., Zanotti, A., Tugnoli, M., Masarati, P., Muscarello, V.: Coupling mid-fidelity aerodynamics and multibody dynamics for the aeroelastic analysis of rotary-wing aircraft configurations. Energies **14**(21), 6979 (2021). https://doi.org/10.3390/en14216979
46. Morino, L.: A general theory of compressible potential aerodynamics. CR 2464, NASA (1974)
47. Hua, Y., Sarkar, T.K.: On SVD for estimating generalized eigenvalues of singular matrix pencil in noise. IEEE Trans. Signal Process. **38**(5), 814–824 (1990). https://doi.org/10.1109/78.55205
48. Pivetta, P., Trezzini, A.A., Favale, M., Lilliu, C., Colombo, A.: Matrix pencil method integration into stabilization diagram for poles identification in rotorcraft and powered-lift applications. In: 45th European Rotorcraft Forum, Warsaw, Poland (2019)
49. Velo, A., Fonte, F., Favale, M., Soal, K., Böswald, M., Volkmar, R., Schwochow, J.: Uncertainty estimation in experimental whirl flutter modes identification. In: Vertical Flight Society's 81st

Annual Forum, Virginia Beach, VA, USA (2025). https://doi.org/10.4050/F-0081-2025-239
50. Adams, B.M., Bohnhoff, W.J., Dalbey, K.R., Ebeida, M.S., Eddy, J.P., Eldred, M.S., Hooper, R.W., Hough, P.D., Hu, K.T., Jakeman, J.D., et al.: Dakota, a multilevel parallel object-oriented framework for design optimization, parameter estimation, uncertainty quantification, and sensitivity analysis: version 6.13 user's manual. Technical report, Sandia National Lab.(SNL-NM), Albuquerque, NM (United States) (2020)
51. Sage, R.M.: The mathematical modelling of ball-joints with friction. Ph.D. thesis, University of Leicester (1987)